

Neural Posterior Regularization for Likelihood-Free Inference

Dongjun Kim^a, Kyungwoo Song^b, Seungjae Shin^a, Wanmo Kang^c, Il-Chul Moon^a, Weonyoung Joo^{d,*}

^aDepartment of Industrial and Systems Engineering, Korea Advanced Institute of Science and Technology (KAIST), Daejeon, Republic of Korea

^bDepartment of Artificial Intelligence, University of Seoul, Seoul, Republic of Korea

^cDepartment of Mathematical Sciences, Korea Advanced Institute of Science and Technology (KAIST), Daejeon, Republic of Korea

^dDepartment of Statistics, Ewha Womans University, Seoul, Republic of Korea

Abstract

A simulation is useful when the phenomenon of interest is either expensive to regenerate or irreproducible with the same context. Recently, Bayesian inference on the distribution of the simulation input parameter has been implemented sequentially to minimize the required simulation budget for the task of simulation validation to the real-world. However, the Bayesian inference is still challenging when the ground-truth posterior is multi-modal with a high-dimensional simulation output. This paper introduces a regularization technique, namely Neural Posterior Regularization (NPR), which enforces the model to explore the input parameter space effectively. Afterward, we provide the closed-form solution of the regularized optimization that enables analyzing the effect of the regularization. We empirically validate that NPR attains the statistically significant gain on benchmark performances for diverse simulation tasks.

Keywords: Likelihood-Free Inference, Simulation Parameter Calibration, Generative Models

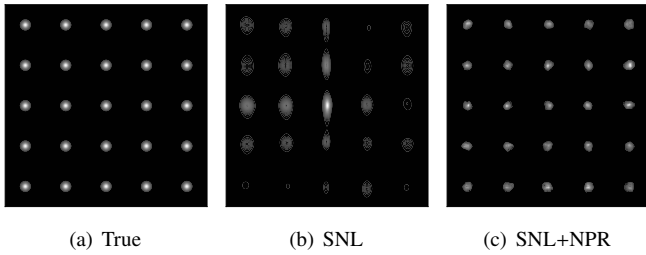


Figure 1: Comparison of (a) the true posterior and the approximate posteriors inferred by (b) SNL and (c) SNL+NPR. We select (θ_1, θ_2) from a uniform distribution on $[0, 1]^2$ and synthetically generate the outcome from a Gaussian distribution $\mathcal{N}([\cos 5\pi\theta_1, \cos 5\pi\theta_2], 0.1\mathbf{I})$ with $\mathbf{x}_o = [0, 0]$.

1. Introduction

Recently, enhanced computing power has motivated the construction of highly complex simulation models. However, these high-resolution simulations achieve high precision only if we calibrate the adjustable simulation input parameters because otherwise, the simulation outcome significantly varies from the real world. The Bayesian inference [1, 2] is one possible yet general framework for such calibration task. The Bayesian inference, however, is challenging because the likelihood function of the simulation is intractable [3] in general.

Recent algorithms on the simulation-based inference, or *likelihood-free inference* [3], parametrizes the model posterior distribution with a neural network. However, not every neural network-based *likelihood-free inference* is advantageous over previous practices in terms of the amount of simulation budget.

Besides, as the simulation complexity increases, the posterior distribution is likely to attain multi-modalities [5], and these factors combine to lead the inference to a highly challenging task. For instance, Fig. 1 illustrates that the inference fails with limited data on a toy simulation with a multi-modal posterior.

We introduce a regularization technique to solve this multi-modal issue, particularly in a high-dimensional case [4]. This regularization is a mixture of the reverse KL divergence and the mutual information that behaves in comparative ways. In the middle rounds of *likelihood-free inference*, the reverse KL regularization encourages the mode-centered dataset because it has the mode-seeking property; and the mutual information regularization estimates the complex posterior within the budget since it captures the rich representation. As the regularization is intractable in its vanilla form, we provide the proxy of the regularization that is tractable, namely Neural Posterior Regularization (NPR). Afterward, we analyze this NPR theoretically by providing the closed-form solution of the regularized loss. Also, we empirically demonstrate its advances under the multi-modal and high-dimensional settings of simulations.

The remainder of this paper is organized as follows. In Section 2, we present the preliminaries of the *likelihood-free inference* and its hurdles. To overcome such difficulties of the current practice, we propose a new regularization in Section 3, and its detailed estimation together with theorems in Section 4. Motivated by the theorems, we suggest an efficient scheduling method for the regularization coefficient in Section 5. Empirical results in various simulations are presented in Section 6.

*Corresponding author

Email address: weonyoungjoo@ewha.ac.kr (Weonyoung Joo)

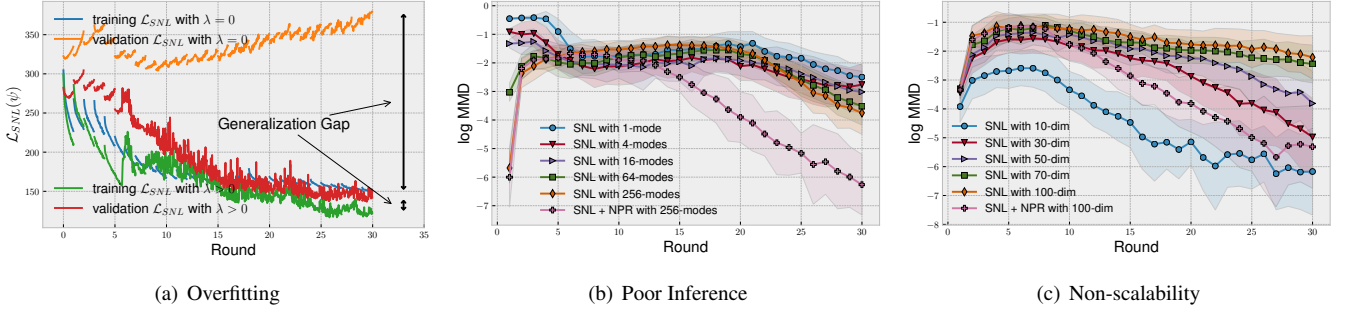


Figure 2: SNL with no regularization ($\lambda = 0$) on SLCP-16 [4] suffers from (a) large generalization gap (b) inaccurate posterior estimation on multi-modal posterior (c) slow learning on high dimensional output.

2. Preliminary

2.1. Problem Definition

The evaluation on the likelihood of $p_{sim}(\mathbf{x}|\theta)$ in a simulation is not allowed because a simulation is fundamentally a data-generation descriptive process. The purpose of *likelihood-free inference* is estimating the posterior distribution $p_{sim}(\theta|\mathbf{x} = \mathbf{x}_o)$, where \mathbf{x}_o is a one-shot real world observation, assuming that the real world with the same context happens only *once*.

2.2. Sequential Likelihood-Free Inference

Recent approaches of *likelihood-free inference* estimate the posterior with the iterative rounds of inference, where the iterative rounds gradually fasten the approximate posterior to the ground-truth posterior. This *sequential* approach is becoming the mainstream in the community of *likelihood-free inference* because the iterative optimization saves the simulation budgets by orders of magnitude [6].

Initial round. The sequential likelihood-free inference gathers simulation inputs from the prior distribution $p(\theta)$, the uniform distribution on the input space. A collection of simulation input-output pairs constructs a dataset for the initial round $\mathcal{D}_1 = \{(\theta_{1,j}, \mathbf{x}_{1,j})\}_{j=1}^N$, where each $\mathbf{x}_{1,j}$ is the simulation output corresponding to $\theta_{1,j}$, i.e., $\mathbf{x}_{1,j} \sim p_{sim}(\mathbf{x}|\theta_{1,j})$. The approximate posterior on the initial round with \mathcal{D}_1 is trained by either one of the inference algorithms described in Section 2.3.

Next rounds. The new simulation inputs are drawn from a proposal distribution $\theta_{r,j} \sim p_r(\theta)$. The proposal distribution is the approximate posterior at the last round $p_r(\theta) := q_{r-1}(\theta|\mathbf{x}_o)$. The algorithm accumulates the newly simulated data into the training dataset as $\mathcal{D}_r \leftarrow \mathcal{D}_{r-1} \cup \{(\theta_{r,j}, \mathbf{x}_{r,j})\}_{j=1}^N$, where $\mathbf{x}_{r,j} \sim p(\mathbf{x}|\theta_{r,j})$, and approximates the posterior.

2.3. Inference Algorithms

Neural Likelihood. Papamakarios et al. [1] estimates the likelihood $p(\mathbf{x}|\theta)$ with a (conditional) neural network $q_\psi(\mathbf{x}|\theta)$ parametrized by ψ . Given $\tilde{p}_r(\theta) := \frac{1}{r} \sum_{s=1}^r p_s(\theta)$ is the cumulative input distribution, the optimization loss becomes

$$\begin{aligned} \mathcal{L}_{SNL}(\psi) &= -\mathbb{E}_{(\theta, \mathbf{x}) \sim \tilde{p}_r(\theta) p_{sim}(\mathbf{x}|\theta)} [\log q_\psi(\mathbf{x}|\theta)] \\ &= D_{KL}(\tilde{p}_r(\theta) p_{sim}(\mathbf{x}|\theta) \| \tilde{p}_r(\theta) q_\psi(\mathbf{x}|\theta)) + C, \end{aligned}$$

where C is a constant irrelevant to ψ . The optimal neural likelihood $q_{\psi^*}(\mathbf{x}|\theta)$ matches to the ground-truth likelihood $p_{sim}(\mathbf{x}|\theta)$ if the training dataset sufficiently covers the space of input parameters. The approximate posterior of this Sequential Neural Likelihood (SNL) is given as the unnormalized form by $q_r(\theta|\mathbf{x}_o) \propto p(\theta) q_\psi(\mathbf{x}_o|\theta)$ with the trained ψ .

Neural Posterior. Greenberg et al. [2] directly estimates the posterior $p_{sim}(\theta|\mathbf{x})$ with a neural network $q_\phi(\theta|\mathbf{x})$ parametrized by ϕ . The optimization loss of this Automatic Posterior Transformation (APT) is the (normalized) negative log-posterior $\mathcal{L}_{APT}(\phi) = -\mathbb{E}_{(\theta, \mathbf{x}) \sim \tilde{p}_r(\theta) p_{sim}(\mathbf{x}|\theta)} [\log \frac{q_\phi(\theta|\mathbf{x})}{Z_\phi(\mathbf{x})}]$, which is equivalent to the KL divergence $D_{KL}(\tilde{p}_r(\theta) p_{sim}(\mathbf{x}|\theta) \| \tilde{p}_r(\theta) \frac{q_\phi(\theta|\mathbf{x})}{p(\theta)} \frac{\tilde{p}_r(\mathbf{x})}{Z_\phi(\mathbf{x})})$. Here, $Z_\phi(\mathbf{x}) = \int q_\phi(\theta|\mathbf{x}) \frac{\tilde{p}_r(\theta)}{p(\theta)} d\theta$ is the normalizing constant and $\tilde{p}_r(\mathbf{x}) = \mathbb{E}_{\tilde{p}_r(\theta)} [p_{sim}(\mathbf{x}|\theta)]$ is the outcome distribution expected by $\tilde{p}_r(\theta)$.

2.4. Issues of Neural Likelihood

Despite the equivalence of the optimal neural likelihood to the ground-truth likelihood, SNL is under severe overfitting, as evidenced in Fig. 2-(a). This overfitting prevents the accurate estimation of the neural likelihood, and the approximate posterior $q_\psi(\theta|\mathbf{x}_o) \propto p(\theta) q_\psi(\mathbf{x}_o|\theta)$ becomes inaccurate in Fig. 2-(b) and Fig. 3-(b). This immatured inference at each round gives an inaccurate signal when we sample the next batch of the simulation run, and this feedback loop eventually leads the inference failure within a limited simulation budget. Furthermore, SNL is not scalable to the outcome dimension in Fig. 2-(c).

3. Regularization on Training the Neural Likelihood

To resolve the aforementioned issues, we introduce a constrained problem

$$\text{minimize } \mathcal{L}_{SNL}(\psi) \text{ subject to } F(\psi) \leq C, \quad (1)$$

where C is a constant that restricts the class of neural likelihood to $\mathcal{F} = \{q_\psi : F(\psi) \leq C\}$. The Lagrangian of the problem is

$$\mathcal{L}_\lambda(\psi) = \mathcal{L}_{SNL}(\psi) + \lambda F(\psi),$$

where $\lambda > 0$ is the regularization magnitude.

To determine a specific form of the constraint, recall that the optimization loss is the forward KL divergence between

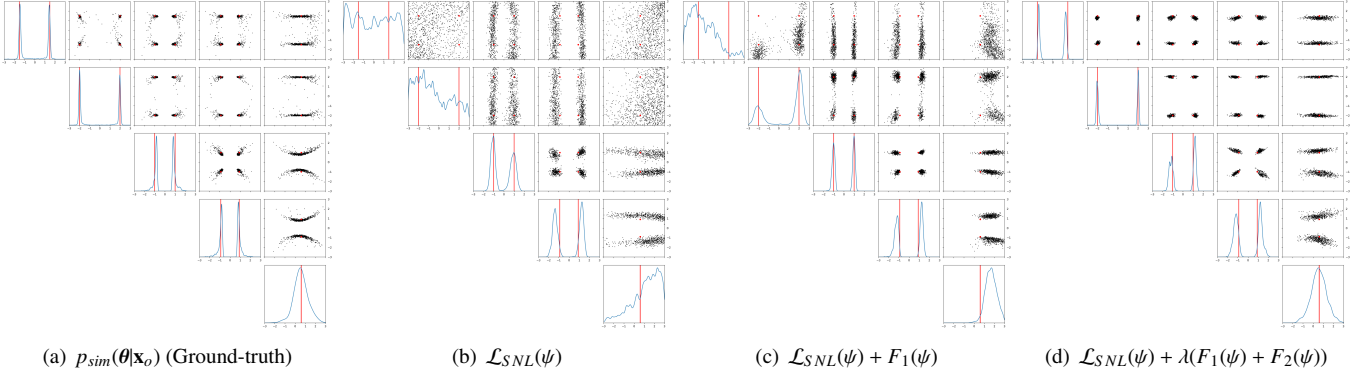


Figure 3: Comparison of (a) the ground-truth posterior $p_{sim}(\theta|\mathbf{x}_o)$ and the approximate posterior $q_\psi(\theta|\mathbf{x}_o)$ inferred by (b) SNL loss $\mathcal{L}_{SNL}(\psi)$, (c) SNL with the reverse KL regularization $\mathcal{L}_{SNL}(\psi) + \lambda F_1(\psi)$, and (d) SNL with our regularization $\mathcal{L}_{SNL}(\psi) + \lambda(F_1(\psi) + F_2(\psi))$ on SLCP-16 [4]. The diagonal boxes represent marginal distributions for each parameter input, and the off-diagonal boxes represent the random samples from the posterior distribution as black dots, projected into the two-dimensional subspace for each pair of parameter inputs. The red dots and lines represent the ground-truth input parameters. We apply the adversarial method from Nowozin et al. [7] to estimate F_1 in (c); we use the proposed $F(\psi, \phi)$ to estimate $F(\psi)$ in (d). We use the exponentially decaying λ , see Section 5 for the details.

the true joint distribution $\tilde{p}_r(\theta)p_{sim}(\mathbf{x}|\theta)$ and the modeled joint distribution $\tilde{p}_r(\theta)q_\psi(\mathbf{x}|\theta)$. Due to the mode-covering property [8] of the forward KL divergence, the approximate posterior $q_\psi(\theta|\mathbf{x}_o)$ becomes inaccurate to the ground-truth posterior $p_{sim}(\theta|\mathbf{x}_o)$, as in Fig. 3-(b) without penalizing the mode-covering. Specifically, we observe that θ samples out of modes hardly contribute to the inference quality, so class \mathcal{F} consisting of the mode concentrated distributions would have merits in the inference. In addition, the rich representation power would significantly mitigate the overfitting issue. Summing together, we design the constraint as

$$F(\psi) = F_1(\psi) + F_2(\psi),$$

where F_1 forces the posterior to exploit its modes and F_2 is for the better representation with the limited amount of data.

As the reverse KL has the *mode-seeking* property [9], we define F_1 by

$$F_1(\psi) = D_{KL}(\tilde{p}_r(\theta)q_\psi(\mathbf{x}|\theta) \parallel \tilde{p}_r(\theta)p_{sim}(\mathbf{x}|\theta)).$$

The mode-seeking property of the reverse KL strongly penalizes a dispersive distribution with non-zero values on the intermediate region between modes, whereas the forward KL $\mathcal{L}_{SNL}(\psi)$ prefers a mode-covering distribution. Therefore, the weighted loss $\mathcal{L}_{SNL}(\psi) + \lambda F_1(\psi)$ mixes two extremes in a unified optimization loss by taking both contrastive properties inherited from forward and reverse KLs. In other words, the weighted divergence searches distributions with accurate modes while retaining the mode diversity. The weight of λ controls the trade-off between the exploration and exploitation effects.

On the other hand, we propose to utilize the mutual information in place of F_2 constraint by

$$F_2(\psi) = -\mathbb{I}(\theta, \mathbf{x}) = -D_{KL}(\tilde{p}_r(\theta)q_\psi(\mathbf{x}|\theta) \parallel \tilde{p}_r(\theta)\tilde{q}_\psi(\mathbf{x})),$$

where $\tilde{q}_\psi(\mathbf{x}) := \mathbb{E}_{\tilde{p}_r(\theta)}[q_\psi(\mathbf{x}|\theta)]$ is the expected neural likelihood. The maximum mutual information principle enforces the coupling of θ and \mathbf{x} with the neural likelihood $q_\psi(\mathbf{x}|\theta)$ to be informative. This maximum principle is particularly effective in

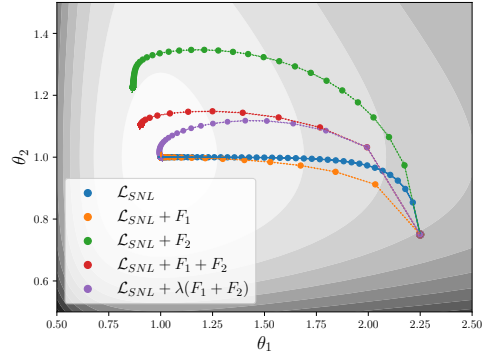


Figure 4: Optimization trajectories for various loss candidates in a toy example. Either of \mathcal{L}_{SNL} and $\mathcal{L}_{SNL} + F_1$ converges to the optimum, where F_1 (reverse KL) encourages the faster convergence. The regularization with F_2 blocks the learning curve to converge to the global optimum, but the curve of $\mathcal{L}_{SNL} + \lambda(F_1 + F_2)$ converges to the global optimum if we anneal λ exponentially decaying.

resolving the mode collapse problem [10] as well as capturing the rich representation on high dimensions [11].

We investigate the effect of our regularization in a toy case with a tractable likelihood of $p(x_1, x_2) = \mathcal{N}(x_1; 0, 1)\mathcal{N}(x_2; x_1, 1)$. If the model likelihood is $q(x_1, x_2) = \mathcal{N}(x_1, 0, \theta_1^2)\mathcal{N}(x_2; x_1, \theta_2^2)$, we can derive closed-forms of \mathcal{L}_{SNL} , F_1 , and F_2 :

$$\begin{aligned} \mathcal{L}_{SNL} &= \log \theta_1 + \log \theta_2 + \frac{\theta_1^2 + \theta_2^2}{2\theta_1^2\theta_2^2}, \\ F_1 &= -\log \theta_1 - \log \theta_2 + \frac{\theta_1^2 + \theta_2^2}{2} - 1, \\ F_2 &= \frac{1}{2} \log \theta_1^2 + \theta_2^2 - \log \theta_2. \end{aligned}$$

In this toy example, we optimize θ_1 and θ_2 with respect to the given losses, and mutual information seems to be redundant for the optimization in Fig. 4. However, it turns out that mutual information is key to the better convergence when F_1 and F_2 are intractable.

We show how F_2 affects the inference on SLCP-16 [4] with intractable F_1 and F_2 . As F_1 is intractable to calculate, we use adversarial training [7] for the scalable estimation at the cost

of training instability. Combined with the mutual information, however, we could avoid using adversarial training to estimate $F(\psi)$, and Fig. 3 shows that SNL with our regularization outperforms SNL regularized by F_1 . Quantitatively, we measure the relative mutual information by

$$\mathbb{I}_{rel}(r) := \frac{D_{KL}(\tilde{p}_r(\theta)q_\psi(\mathbf{x}|\theta)\|\tilde{p}_r(\theta)\tilde{q}_\psi(\mathbf{x}))}{D_{KL}(\tilde{p}_r(\theta)p_{sim}(\mathbf{x}|\theta)\|\tilde{p}_r(\theta)\tilde{p}_{sim}(\mathbf{x}))},$$

where $\tilde{p}_{sim}(\mathbf{x}) = \mathbb{E}_{\tilde{p}_r(\theta)}[p_{sim}(\mathbf{x}|\theta)]$. This relative mutual information satisfies $\mathbb{I}_{rel}(r) = 1$ if and only if the neural likelihood $q_\psi(\mathbf{x}|\theta)$ exactly matches the ground-truth likelihood $p_{sim}(\mathbf{x}|\theta)$. In Fig. 5, we compare three loss candidates that converge to the global optimum of Fig. 4: \mathcal{L}_{SNL} , $\mathcal{L}_{SNL} + F_1$, and $\mathcal{L}_{SNL} + \lambda(F_1 + F_2)$. Fig. 5 shows that \mathcal{L}_{SNL} regularized by $F_1 + F_2$ with proper choice of regularization coefficient λ is most close to the dotted line of $q_\psi(\mathbf{x}|\theta) = p_{sim}(\mathbf{x}|\theta)$ among all.

4. Neural Posterior Regularization

4.1. Unified Estimation of Reverse KL and Mutual Information

While $F = F_1 + F_2$ is designed to avoid the inefficient feed-back loop mentioned in Section 2.4, the constraint F cannot be tractably computed in general. Therefore, we introduce a method to approximate the constraint. To begin with, recall that the neural posterior loss is

$$\mathcal{L}_{APT}(\phi) = -\mathbb{E}_{\tilde{p}_r(\theta)p_{sim}(\mathbf{x}|\theta)} \left[\log \frac{q_\phi(\theta|\mathbf{x})}{Z_\phi(\mathbf{x})} \right].$$

By replacing the expected distribution of \mathcal{L}_{APT} from $\tilde{p}_r(\theta)p_{sim}(\mathbf{x}|\theta)$ to $\tilde{p}_r(\theta)q_\psi(\mathbf{x}|\theta)$, the loss \mathcal{L}_{APT} transforms to

$$F(\psi, \phi) = -\mathbb{E}_{\tilde{p}_r(\theta)q_\psi(\mathbf{x}|\theta)} \left[\log \frac{q_\phi(\theta|\mathbf{x})}{Z_\phi(\mathbf{x})} \right]. \quad (2)$$

When the neural posterior satisfies $q_{\phi^*}(\theta|\mathbf{x}) = p_{sim}(\theta|\mathbf{x})$ and $Z_{\phi^*}(\mathbf{x}) = \frac{\tilde{p}_r(\mathbf{x})}{p_{sim}(\mathbf{x})}$ for $p_{sim}(\mathbf{x}) = \mathbb{E}_{p(\theta)}[p_{sim}(\mathbf{x}|\theta)]$, Eq. 2 reduces to

$$F(\psi, \phi^*) = -\mathbb{E}_{\tilde{p}_r(\theta)q_\psi(\mathbf{x}|\theta)} \left[\log \frac{p_{sim}(\theta|\mathbf{x})p_{sim}(\mathbf{x})}{\tilde{p}_r(\mathbf{x})} \right].$$

Then, Theorem 1 proves that $F(\psi, \phi^*)$ is the proxy of the regularization of $F(\psi)$.

Theorem 1. $F(\psi, \phi^*)$ is decomposed into $F(\psi, \phi^*) = F(\psi) - R(\psi)$, up to a constant, where $R(\psi)$ is the residual term given by $R(\psi) = D_{KL}(\tilde{q}_\psi(\mathbf{x})\|\tilde{p}_r(\mathbf{x}))$.

Proof. We have

$$\begin{aligned} F(\psi, \phi^*) &= -\mathbb{E}_{\tilde{p}_r(\theta)q_\psi(\mathbf{x}|\theta)} \left[\log \frac{p_{sim}(\theta|\mathbf{x})p_{sim}(\mathbf{x})}{\tilde{p}_r(\mathbf{x})} \right] \\ &= \int \int \tilde{p}_r(\theta)q_\psi(\mathbf{x}|\theta) \log \frac{p(\theta)q_\psi(\mathbf{x}|\theta)}{p_{sim}(\theta|\mathbf{x})p_{sim}(\mathbf{x})} d\theta d\mathbf{x} \\ &\quad - \int \int \tilde{p}_r(\theta)q_\psi(\mathbf{x}|\theta) \log \frac{\tilde{p}_r(\theta)q_\psi(\mathbf{x}|\theta)}{\tilde{p}_r(\theta)\tilde{q}_\psi(\mathbf{x})} d\theta d\mathbf{x} \\ &\quad - \int \int \tilde{p}_r(\theta)q_\psi(\mathbf{x}|\theta) \log \frac{\tilde{q}_\psi(\mathbf{x})}{\tilde{p}_r(\mathbf{x})} d\theta d\mathbf{x} \end{aligned}$$

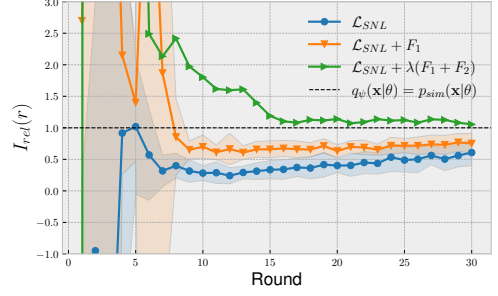


Figure 5: Relative mutual information by inference rounds.

$$\begin{aligned} & - \int \int \tilde{p}_r(\theta)q_\psi(\mathbf{x}|\theta) \log p(\theta) d\theta d\mathbf{x} \\ &= D_{KL}(\tilde{p}_r(\theta)q_\psi(\mathbf{x}|\theta)\|\tilde{p}_r(\theta)p_{sim}(\mathbf{x}|\theta)) \\ &\quad - D_{KL}(\tilde{p}_r(\theta)q_\psi(\mathbf{x}|\theta)\|\tilde{p}_r(\theta)\tilde{q}_\psi(\mathbf{x})) \\ &\quad - D_{KL}(\tilde{q}_\psi(\mathbf{x})\|\tilde{p}_r(\mathbf{x})) + \int \tilde{p}_{sim}(\theta) \log p(\theta) d\theta \\ &= F(\psi) - R(\psi) + C, \end{aligned}$$

where C is irrelevant to ψ . \square

The parameter ϕ estimates the regularization by training the neural posterior, and ψ estimates the ground-truth likelihood by training the neural likelihood. We call $F(\psi, \phi)$ the Neural Posterior Regularization (NPR) since $F(\psi, \phi)$ is computed based on the neural posterior evaluation. Hence, we highlight that our regularization is indeed a unified framework of SNL and APT, and it enjoys the benefits of APT and SNL.

Altogether, we introduce the regularized loss function as

$$\mathcal{L}_\lambda(\psi, \phi) = \mathcal{L}_{SNL}(\psi) + \lambda F(\psi, \phi). \quad (3)$$

This regularized loss approximates the constrained problem of Eq. 1 at the expense of additional neural parameter usage (ϕ). However, it is worth noting that the main interest of *likelihood-free inference* is minimizing the simulation budget rather than reducing the number of neural parameters.

4.2. Optimality Analysis of NPR

The optimal neural likelihood $q_{\psi_\lambda^*}(\mathbf{x}|\theta)$ of $\mathcal{L}_\lambda(\psi, \phi)$ could deviate too far from $p_{sim}(\mathbf{x}|\theta)$. Therefore, we analyze the optimal point of the regularized loss $\mathcal{L}_\lambda(\psi, \phi)$ in Theorem 2.

Theorem 2. Suppose $p_{sim}(\mathbf{x}|\theta)$ and $p(\theta)$ are bounded on a positive interval, $\tilde{p}_r(\theta)$ is bounded below, and $q_\psi(\mathbf{x}|\theta)$ is uniformly upper bounded on ψ . Then $\psi_\lambda^* = \arg \min_\psi \mathcal{L}_\lambda(\psi, \phi)$ satisfies

$$q_{\psi_\lambda^*}(\mathbf{x}|\theta) = \frac{p_{sim}(\mathbf{x}|\theta)}{c(\theta) - \lambda \log \frac{q_\phi(\theta|\mathbf{x})}{Z_\phi(\mathbf{x})}},$$

where $c(\theta)$ is a function of θ that makes $q_{\psi_\lambda^*}(\mathbf{x}|\theta)$ a distribution.

Proof. Suppose $u(\theta, \mathbf{x})$ is a function of (θ, \mathbf{x}) that satisfies $\int u(\theta, \mathbf{x}) d\mathbf{x} = 0$ for any θ , then the function $(q + \epsilon u)(\mathbf{x}|\theta) := q(\mathbf{x}|\theta) + \epsilon u(\theta, \mathbf{x})$ is a distribution on \mathbf{x} for any θ . With the abuse of notation, the difference $\mathcal{L}_\lambda(q_\psi + \epsilon u, q_\phi) - \mathcal{L}_\lambda(q_\psi, q_\phi)$ becomes

$$\mathcal{L}_\lambda(q_\psi + \epsilon u, q_\phi) - \mathcal{L}_\lambda(q_\psi, q_\phi) \quad (4)$$

Table 1: Comparison of performance on SLCP-16 with 100-dimensional and SLCP-256 with 80-dimensional output. The NLTP of SLCP-256 is scaled by 10^{-2} .

Algorithm	SLCP-16			SLCP-256		
	NLTP (\downarrow)	log MMD (\downarrow)	IS (\uparrow)	NLTP (\downarrow)	log MMD (\downarrow)	IS (\downarrow)
SMC-ABC	8.21 \pm 2.36	-1.80 \pm 1.24	13.56 \pm 0.55	75.44 \pm 29.71	-4.48 \pm 0.55	81.69 \pm 7.73
SNPE-A	1.46 \pm 1.72	-4.47 \pm 0.05	2.66 \pm 0.23	39.08 \pm 1.72	-4.55 \pm 0.21	34.74 \pm 3.68
SNPE-B	27.66 \pm 23.83	-2.12 \pm 0.31	1.50 \pm 0.40	140.4 \pm 22.78	-1.83 \pm 0.13	19.43 \pm 0.93
APT (SNPE-C)	3.14 \pm 8.80	-3.27 \pm 0.71	7.39 \pm 4.48	69.04 \pm 93.53	-3.51 \pm 1.24	118.88 \pm 51.30
AALR	0.89 \pm 0.12	-3.57 \pm 0.43	11.22 \pm 3.37	16.19 \pm 1.04	-6.81 \pm 0.68	208.91 \pm 4.33
SNL	4.77 \pm 2.68	-2.53 \pm 0.54	5.34 \pm 3.43	40.40 \pm 11.84	-5.32 \pm 0.65	153.43 \pm 18.40
SNL+NPR	0.55 \pm 0.79	-5.39 \pm 0.94	14.95 \pm 1.08	15.13 \pm 2.65	-6.51 \pm 0.86	211.85 \pm 4.07

Table 2: Comparison of NLTP for the M/G/1 model, the Ricker model, and the Poisson model. Though NLTP on these simulations does not take the structure of the approximate posterior into account, we report this table to comply the previous researches [1].

Algorithm	M/G/1			Ricker			Poisson		
	5	Output Dimension 20	100	13	Output Dimension 20	100	25	Output Dimension 49	361
SMC-ABC	22.54 \pm 17.83	25.48 \pm 22.12	14.85 \pm 18.41	6.77 \pm 7.53	6.02 \pm 7.61	36.12 \pm 18.64	0.92 \pm 1.42	0.58 \pm 1.75	0.00 \pm 0.00
SNPE-A	4.36 \pm 0.43	4.07 \pm 0.49	3.25 \pm 0.61	4.43 \pm 0.20	4.54 \pm 0.49	4.43 \pm 0.18	0.34 \pm 0.48	0.17 \pm 0.42	-3.22 \pm 6.32
SNPE-B	9.30 \pm 0.96	9.85 \pm 0.03	9.89 \pm 0.01	9.79 \pm 0.06	8.67 \pm 1.16	9.96 \pm 0.25	5.44 \pm 5.59	5.59 \pm 4.92	3.47 \pm 4.67
APT (SNPE-C)	-3.49 \pm 0.97	-2.27 \pm 7.14	-3.01 \pm 1.82	-0.62 \pm 0.98	-0.24 \pm 3.86	4.13 \pm 6.16	-11.61 \pm 1.93	-11.61 \pm 2.50	-11.26 \pm 0.96
AALR	-1.18 \pm 0.59	-1.69 \pm 0.51	1.14 \pm 2.08	4.10 \pm 0.51	1.82 \pm 0.77	3.15 \pm 2.55	-6.36 \pm 1.66	-6.25 \pm 0.92	0.28 \pm 0.66
SNL	-3.23 \pm 1.25	-5.58 \pm 1.37	-4.65 \pm 1.30	-1.46 \pm 0.66	-0.41 \pm 1.07	1.44 \pm 6.42	-12.76 \pm 0.99	-12.48 \pm 0.95	-2.36 \pm 7.44
SNL+NPR	-3.86 \pm 0.68	-6.36 \pm 0.78	-5.52 \pm 0.83	-1.78 \pm 0.89	-1.14 \pm 1.25	-0.48 \pm 0.70	-13.31 \pm 1.11	-13.61 \pm 0.83	-5.33 \pm 4.33

$$= -\epsilon \int \int \tilde{p}_r(\theta) u(\theta, \mathbf{x}) \left(\frac{p(\mathbf{x}|\theta)}{q_\psi(\mathbf{x}|\theta)} + \lambda \log \frac{q_\phi(\theta|\mathbf{x})}{Z_\phi(\mathbf{x})} \right) d\theta d\mathbf{x} + o(\epsilon).$$

Therefore, the optimal solution of $\arg \min_{\psi} \mathcal{L}_\lambda(\psi, \phi)$ is where Eq. 4 becomes zero for all $u(\theta, \mathbf{x})$ with $\int u(\theta, \mathbf{x}) d\mathbf{x} = 0, \forall \theta \in \Theta$. By the canonical calculus using the Minkowski and Hölder’s inequalities, we derive that

$$\frac{p_{sim}(\mathbf{x}|\theta)}{q_{\psi_\lambda^*}(\mathbf{x}|\theta)} + \lambda \log \frac{q_\phi(\theta|\mathbf{x})}{Z_\phi(\mathbf{x})} = c(\theta),$$

from Eq. 4 for some function $c(\theta)$ that makes $q_{\psi_\lambda^*}(\mathbf{x}|\theta)$ a distribution. Also, the canonical analysis proves the uniqueness of the optimal distribution, which completes the proof. \square

5. Study on Regularization Coefficient

Searching for the optimal λ would be highly impractical if the simulation budget is strictly limited. Hence, the optimal strategy of λ is required a-priori for *likelihood-free inference*. Fig. 6 illustrates the inference quality by round on SLCP-16/256 [4] with 16/256 modes, respectively. We measure inference quality by the Inception Score (IS) [12], which counts the diversity of the approximate posterior. A higher IS indicates a better inference.

Consistent with the experiment of the toy case in Fig. 4, the multi-round inference in Fig. 6 shows that the inference with $\lambda = 1$ is faster than that of $\lambda = 0$. However, the best λ magnitude differs by SLCP-16 and SLCP-256 with $\lambda = 1$ and $\lambda = 10$, respectively, and this inconsistency by simulation model leads us to propose the λ -scheduling. Motivated by Theorem 2, we propose annealing methods for the λ -scheduling. In Fig. 6,

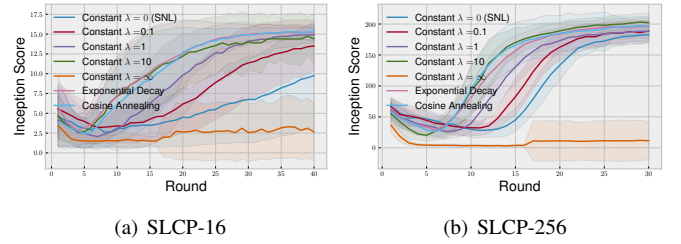


Figure 6: Effect of the regularization coefficient on the inference quality.

either of the exponential decaying and cosine annealing scheduling methods performs as well as the best λ choices, and these adaptive scheduling methods reduce the endeavor of λ search. We choose the exponential decaying strategy by default.

6. Experiments

6.1. Experimental Setup

We experiment with the regularization on a couple of tractable simulations, three science-driven simulation models, and three pre-trained GAN generator models. For the tractable simulations, we utilize the models of the SLCP-family [1], i.e., SLCP-16/256 [4], to test the regularization with highly multi-modal posterior. We use the default setting of SLCP-16/256, except for simulation output dimensions, by doubling from 50 to 100 on SLCP-16 and 40 to 80 on SLCP-256. Next, we experiment with realistic simulations without the tractable likelihood. The simulations are 1) the M/G/1 model [1] from the queuing theory; 2) the Ricker model [13] from the field of ecology; and 3) the Poisson model [14] in the field of physics. We experiment with these simulations with three output dimension variations to test the robustness in high-dimensional cases (see Table 2). Other than

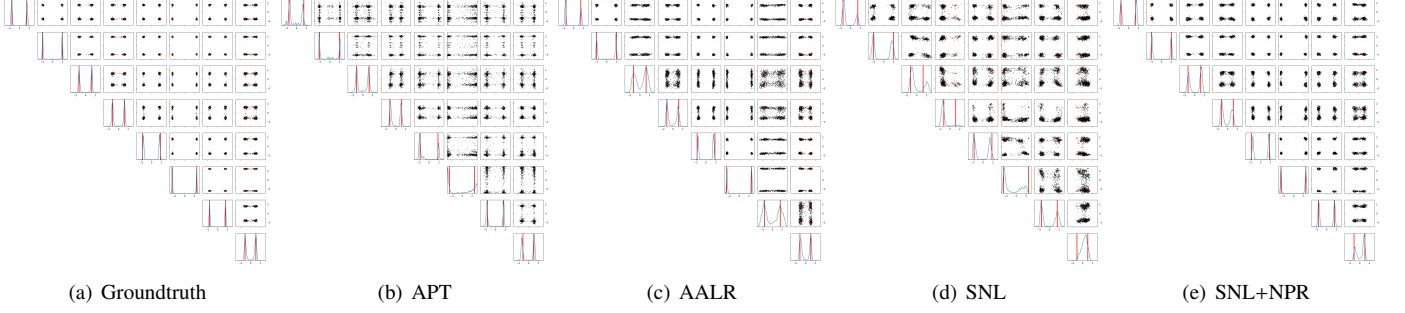


Figure 7: Comparison of the approximate posterior distributions on SLCP-256.

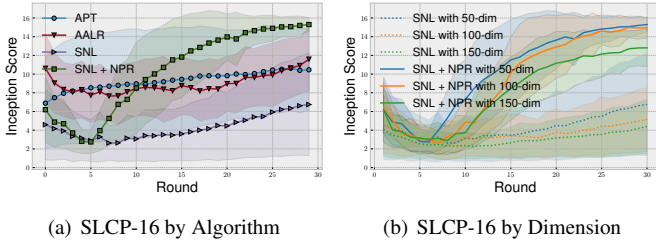


Figure 8: IS by round on (a) baselines of 50-dim output and (b) varying dimensions.

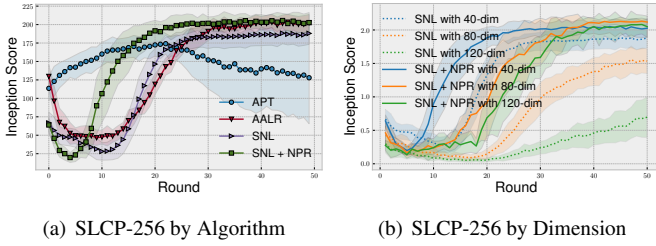


Figure 9: IS by round with (a) baselines of 40-dim output and (b) varying dimensions.

the dimension, we comply with the original setup. Lastly, we experiment with the pre-trained GAN generator [15] for the image restoration task. We test on MNIST [16], Fashion MNIST [17], and SVHN [18].

We use the Neural Spline Flow [19] for modeling both neural likelihood and neural posterior. We assume that the simulation budget per round is 100 for all but M/G/1 with 20. We run 50 rounds of inference for SLCP-256, 30 for SLCP-16, M/G/1, Ricker, and Poisson, and 15 for GAN generator models. We compare the regularized SNL with SMC-ABC [20], SNPE-A [3], SNPE-B [21], APT [2], AALR [22], and SNL [1]. For the performance metrics, we use Maximum Mean Discrepancy (MMD) [23], IS, Median distance (MEDDIST) [24], Simulation-Based Calibration (SBC) [1], as well as Negative Log-likelihood of True Parameters (NLTP) [24]. We release the code at https://github.com/Kim-Dongjun/Neural_Posterior_Regularization.

6.2. Experimental Result

Tables 1 and 2 present the quantitative results of each simulation with 30 replications. $N = 100$ for all but M/G/1 with

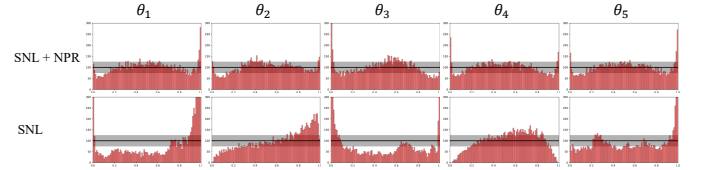


Figure 10: SBC after 10 rounds of inference on the MNIST experiment.

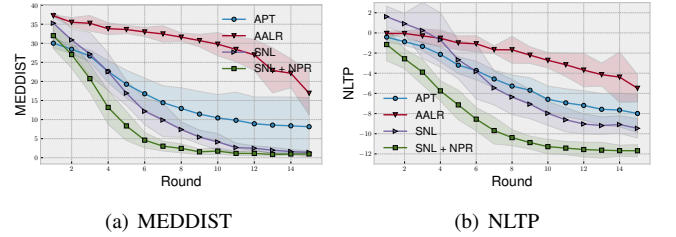


Figure 11: MEDDIST and NLTP on the MNIST experiment.

$N = 20$, and run the 50 inference rounds. The regularized algorithm shows robustness and finds most modes compared to the baselines. Fig. 7 presents the approximate posterior. It shows that the regularized SNL performs the best out of baselines with a limited simulation budget. Empirically, with $N = 100$, the regularized SNL requires nearly 20 rounds to capture all modes.

Figures 8 and 9 illustrate the performance by rounds. The regularized SNL consistently outperforms the baselines in terms of the IS. In particular, the regularized SNL could be framed as a mix of APT and SNL in its loss design, but the regularized SNL outperforms both APT and SNL. Fig. 8-(b) and Fig. 9-(b) empirically demonstrate that the regularization gives robust inference across diverse dimensions.

Figure 12 shows the image restoration from a single shot of the given image on MNIST, Fashion MNIST, and SVHN. The regularized SNL significantly outperforms the baselines on all tasks regarding the generated sample quality. In contrast to SNL, the regularized SNL finds multiple modes in Fig. 13. Quantitatively, we compare the regularized SNL with baselines in Fig. 10 and Fig. 11 on the MNIST experiment.

7. Conclusion

This paper proposes a new regularization for *likelihood-free inference*. We approximate this regularization as NPR, and the

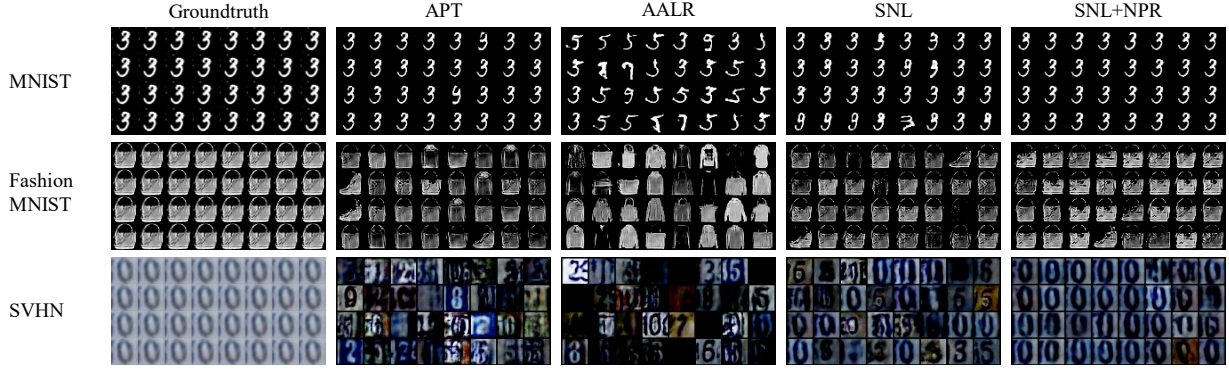


Figure 12: Image restoration based on the given groundtruth image.

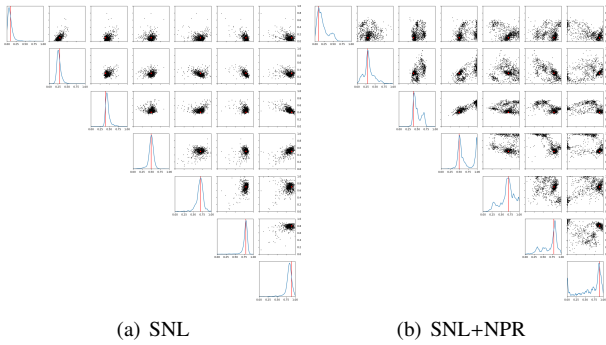


Figure 13: Approximate posterior on Fashion MNIST.

regularized SNL can be interpreted as the joint combination of APT and SNL in a unified framework. The optimality of the regularized SNL is driven as a closed-form solution, and the tuning of the regularization magnitude does not require additional cost. The experimental results support that the proposed regularization method takes benefits from both SNL and APT.

References

- [1] G. Papamakarios, D. Sterratt, I. Murray, Sequential neural likelihood: Fast likelihood-free inference with autoregressive flows, in: The 22nd International Conference on Artificial Intelligence and Statistics, 2019, pp. 837–848.
- [2] D. Greenberg, M. Nonnenmacher, J. Macke, Automatic posterior transformation for likelihood-free inference, in: International Conference on Machine Learning, 2019, pp. 2404–2414.
- [3] G. Papamakarios, I. Murray, Fast ϵ -free inference of simulation models with bayesian conditional density estimation, in: Advances in Neural Information Processing Systems, 2016, pp. 1028–1036.
- [4] D. Kim, K. Song, Y. Kim, Y. Shin, I.-C. Moon, Sequential likelihood-free inference with implicit surrogate proposal, arXiv preprint arXiv:2010.07604 (2020).
- [5] A. Aushev, H. Pesonen, M. Heinonen, J. Corander, S. Kaski, Likelihood-free inference with deep gaussian processes, arXiv preprint arXiv:2006.10571 (2020).
- [6] K. Cranmer, J. Brehmer, G. Louppe, The frontier of simulation-based inference, Proceedings of the National Academy of Sciences (2020).
- [7] S. Nowozin, B. Cseke, R. Tomioka, f-gan: Training generative neural samplers using variational divergence minimization, in: Advances in neural information processing systems, 2016, pp. 271–279.
- [8] M. Zhang, T. Bird, R. Habib, T. Xu, D. Barber, Variational f-divergence minimization, arXiv preprint arXiv:1907.11891 (2019).
- [9] B. Poole, A. A. Alemi, J. Sohl-Dickstein, A. Angelova, Improved generator objectives for gans, arXiv preprint arXiv:1612.02780 (2016).
- [10] K. S. Lee, N.-T. Tran, N.-M. Cheung, Infomax-gan: Improved adversarial image generation via information maximization and contrastive learning, in: Proceedings of the IEEE/CVF Winter Conference on Applications of Computer Vision, 2020, pp. 3942–3952.
- [11] P. Bachman, R. D. Hjelm, W. Buchwalter, Learning representations by maximizing mutual information across views, in: Advances in Neural Information Processing Systems, 2019, pp. 15535–15545.
- [12] T. Salimans, I. Goodfellow, W. Zaremba, V. Cheung, A. Radford, X. Chen, Improved techniques for training gans, in: Advances in neural information processing systems, 2016, pp. 2234–2242.
- [13] M. U. Gutmann, J. Corander, Bayesian optimization for likelihood-free inference of simulator-based statistical models, The Journal of Machine Learning Research 17 (2016) 4256–4302.
- [14] D. Kim, W. Joo, S. Shin, I.-C. Moon, Adversarial likelihood-free inference on black-box generator, arXiv preprint arXiv:2004.05803 (2020).
- [15] M. Arjovsky, S. Chintala, L. Bottou, Wasserstein generative adversarial networks, in: International conference on machine learning, PMLR, 2017, pp. 214–223.
- [16] Y. LeCun, L. Bottou, Y. Bengio, P. Haffner, Gradient-based learning applied to document recognition, Proceedings of the IEEE 86 (1998) 2278–2324.
- [17] H. Xiao, K. Rasul, R. Vollgraf, Fashion-mnist: a novel image dataset for benchmarking machine learning algorithms, arXiv preprint arXiv:1708.07747 (2017).
- [18] Y. Netzer, T. Wang, A. Coates, A. Bissacco, B. Wu, A. Y. Ng, Reading digits in natural images with unsupervised feature learning (2011).
- [19] C. Durkan, A. Bekasov, I. Murray, G. Papamakarios, Neural spline flows, in: Advances in Neural Information Processing Systems, 2019, pp. 7511–7522.
- [20] S. A. Sisson, Y. Fan, M. M. Tanaka, Sequential monte carlo without likelihoods, Proceedings of the National Academy of Sciences 104 (2007) 1760–1765.
- [21] J.-M. Lueckmann, P. J. Goncalves, G. Bassetto, K. Ocal, M. Nonnenmacher, J. H. Macke, Flexible statistical inference for mechanistic models of neural dynamics, in: Neural Information Processing Systems (NIPS 2017), 2018.
- [22] J. Hermans, V. Begy, G. Louppe, Likelihood-free mcmc with amortized approximate ratio estimators, in: International Conference on Machine Learning, 2020.
- [23] B. K. Sriperumbudur, A. Gretton, K. Fukumizu, B. Schölkopf, G. R. Lanckriet, Hilbert space embeddings and metrics on probability measures, The Journal of Machine Learning Research 11 (2010) 1517–1561.
- [24] J.-M. Lueckmann, J. Boelts, D. Greenberg, P. Goncalves, J. Macke, Benchmarking simulation-based inference, in: International Conference on Artificial Intelligence and Statistics, PMLR, 2021, pp. 343–351.